Catalysis Today 149 (2010) 212–217

Contents lists available at ScienceDirect

Catalysis Today

journal homepage: www.elsevier.com/locate/cattod

Structural features of binary microporous zeolite composite Y-Beta and its hydrocracking performance

Xiwen Zhang [a,b], Qun Guo [a], Bo Qin [b], Zhizhi Zhang [b], Fengxiang Ling [b], Wanfu Sun [b], Ruifeng Li [a,*]

[a] Key Laboratory of Coal Science and Technology, MOE, Institute of Special Chemicals, Taiyuan University of Technology, Taiyuan 030024, China
[b] Fushun Research Institute of Petroleum and Petrochemicals, SINOPEC, Fushun 113001, China

ARTICLE INFO

Keywords:
Zeolite composite
Structural feature
Acid catalyst
Hydrocracking

ABSTRACT

Y-Beta zeolite composites denoted as HS-FBZ (High-Silica-Faujasite-Beta-Zeolite) were synthesized hydrothermally using high silica Y as precursor and characterized by XRD, N_2 adsorption, SEM, HRTEM, NH_3-TPD and FT-IR spectra of pyridine. The results reveal that the different ratios of Y and Beta zeolites in the composites induced the change of surface areas, pore diameters and acid properties of HS-FBZ, and the extended Beta layers on the zeolite Y surface were observed. The composite exhibited an excellent hydrocracking activity for heavy oil. Compared with the corresponding physical mixture of Y and Beta zeolites, the zeolite composite as a hydrocracking catalyst for vacuum gas oil increased the heavy naphtha yield by 5.61 wt% and the jet fuel yield by 11.52 wt%.

Zeolite Y as a catalytic material was widely studied because of its appropriate pore structure, acidity, thermal and hydrothermal stability in petroleum refining [1–6]. On the other hand, the high acid density of zeolite Y facilitates the deposition of carbon in its channels, especially on its external surface, which causes a blockage of the channels and an untimely deactivation of the catalyst in the catalytic cracking. Many studies have been conducted to modify zeolite Y, which gives rise to improved surface property of the zeolite so as to obtain a reasonable distribution of acidity [7–9]. Similarly, significant attentions had been focused on zeolite Beta as a result of its high Si/Al ratio and hydroisomerization activity, low hydrogen-transfer capacity and catalytic deactivation, and easy availability in petrochemical processing [10–12]. Previous studies focused mainly on properties and applications of the two zeolites in hydrocracking [5,12–14]. Recently, with the appearance of zeolite composites, such as ZSM-5/Y [15,16], MCM-41-Beta [17], and MCM-41/Y [18], many researchers had paid attention to the study of the composites in hydrocracking and FCC processes [15,16], in which the composites show the advantage over single component because of the combination of two kinds of molecular sieves. Li and his co-workers synthesized a High-Silica-Faujasite-Beta-Zeolite composite (HS-FBZ) using high silica Y as precursor [19,20]. However, the understanding on the structure and property of the zeolite composite is still very limited. In the present paper, the zeolite composite HS-FBZ was synthesized in the same way and further investigated to reveal its physico-chemical and hydrocracking properties, as well as the correlation between them. The hydrocracking activity of HS-FBZ was investigated and compared with that of physical mixture of Y and Beta zeolites.

1. Experimental

1.1. Synthesis of HS-FBZ composite

The HS-FBZ composite zeolite was prepared hydrothermally in a Teflon-lined autoclave under static condition. Typically, 7.2 g of Y zeolite powder was treated in 35 mL of 0.1 mol/L NaOH aqueous solution at 80 °C for 12 h [21], then 5.8 g of tetraethylammonium bromide (TEABr) and 2 mL of NH_4OH were added to the mixture, and the pH value of the system was adjusted to 13 by adding 1 mol/L H_2SO_4. The resultant mixture was stirred at room temperature for 0.5 h, subsequently 21 mL of silica sol was added slowly under vigorous stirring. Finally, the mixture was heated at 140 °C for 5–9 days. The synthesized product was filtered, washed with distilled water to pH < 8.0, and dried at 100 °C overnight. The as-synthesized sample was calcined at 500 °C for 5 h under air atmosphere to remove the organic template. The heating rate was controlled at 2 °C/min. By the same procedure, three HS-FBZ zeolite composites with different amounts of Beta and Y zeolites were obtained, of which the composites including 20 wt%, 40 wt% and 60 wt% Beta zeolite are denoted as HS-FBZ-20, HS-FBZ-40, HS-FBZ-60, respectively. The three composite zeolites have almost the same Si/Al ratios, as determined by chemical analysis, which are 10.91, 10.89, 10.63, respectively. The calcined samples were treated repeatedly three times with 1 mol/L NH_4NO_3 solution at

* Corresponding author. Fax: +86 351 6010121.
E-mail address: ruifeng_li@hotmail.com (R. Li).

0920-5861/$ – see front matter © 2009 Elsevier B.V. All rights reserved.
doi:10.1016/j.cattod.2009.11.005

80 °C for 1 h, filtered and washed with deionized water, and finally calcined at 500 °C for 5 h under air atmosphere to give the H-form of HS-FBZ.

1.2. Catalyst preparation

For hydrocracking reaction, a bifunctional catalyst was prepared, in which the H-form zeolite composite HS-FBZ was used as the support, Ni–Mo as the active components, pseudo-boehmite and amorphous silica–alumina as the binders. The catalyst preparation procedure was as follows: HS-FBZ, pseudo-boehmite and amorphous silica–alumina (10–20 wt%) were mixed by grinding, blended by adding distilled water, and extruded to get the catalyst carrier. The bifunctional catalyst was prepared by stepwise impregnation of the carrier with the solution of $(NH_4)_6Mo_7O_{24}$ (Beijing Chemical Co., PR China) and $Ni(NO_3)_2$ (Beijing Chemical Co., PR China). After every carrier impregnation step, the resulting solids were dried at 110 °C for 3 h. The final solid samples were then calcined at 500 °C for 4 h.

1.3. Characterization of HS-FBZ composite

XRD patterns of the samples were recorded using a Rigaku Dmax X-ray diffractometer, Ni-filtered Cu Kα, 40 kV and 80 mA. A working plot was obtained by plotting the intensity of the diffraction peak at $2\theta = 6.16$ versus the mass fraction of Y zeolite by measuring a series of physical mixtures with known mass fractions of Y zeolite. The mass fraction of Y zeolite in the composite HS-FBZ can be estimated from the intensity of the XRD diffraction peak at $2\theta = 6.16$, which is the characteristic peak of Y zeolite. N_2 adsorption–desorption isotherms were obtained at liquid nitrogen temperature on a Micromeritics ASAP2400 apparatus. The mesoporous structure was analyzed from desorption branch of the isotherm by the Barrett–Joyner–Halenda (BJH) method, and the microporous structure was obtained from the *t*-plot analysis of the adsorption branch of the isotherm. Infrared spectra were obtained on a Bio-Rad spectrometer in KBr pellets in the range of 400–1600 cm^{-1}. Crystal morphology and size were determined using a JSM-6301F scanning electron microscope (SEM). X-ray energy dispersive spectroscopy was carried out on Oxford-Link ISIS. TEM images of the prepared materials were captured in a Tecnai G220 field emission electron microscope. Samples were prepared by dispersing the powder in methanol via sonication for about 20 min followed by evaporation on a 300 mesh continuous carbon film TEM grid. The acidity of H-form HS-FBZ was measured by ammonia temperature-programmed desorption technique (NH_3-TPD) on a chemical adsorption instrument Micromeritics 2910. The sample was outgassed at 500 °C for 1 h under He flow and then NH_3 was adsorbed at 100 °C until saturation. Desorption of the adsorbed ammonia began from 100 °C to 500 °C by 10 °C/min after the sample was purged by He. The acid types (i.e. Brønsted or Lewis type) were recorded on an FT-IR spectrometer by in situ pyridine adsorption.

1.4. Catalytic test

The catalytic experiments were carried out on a standard micro-activity test unit (MAT). Iranian vacuum gas oil (VGO) was employed as the feedstock. Reaction conditions were as follows: total pressure = 15.7 MPa, WHSV = 1.5 h^{-1}, and H_2/hydrocarbon molar ratio = 1500/1. Two temperatures were adopted, 385 °C and 382.5 °C. The product was distillated to produce the following fractions: light naphtha, heavy naphtha, gasoline, diesel oil, and tail oil. The product distribution, gasoline group and octane number were off-line analyzed on a gas chromatograph. The coke on catalyst was measured with a coke analyzer.

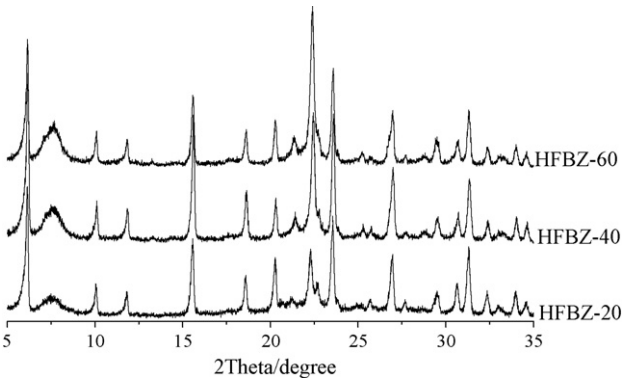

Fig. 1. XRD patterns of HS-FBZ composites.

2. Results and discussion

Fig. 1 shows the XRD patterns of the zeolite composites HS-FBZ. The characteristic peaks corresponding to zeolites Y and Beta can be observed together, indicating the co-existence of Y and Beta zeolite phases in the composite HS-FBZ. The analysis by XRD also shows that the zeolite composite HS-FBZ resulting from the intergrowth of zeolites Y and Beta was obtained with high crystallinity. It is interesting that the peak intensities of high silica Y zeolite phase in the three composites changed only slightly, the peak intensities of Beta zeolite phase at 7.5 and 22.4° increased gradually with the increasing crystallization time. As a result an extended Beta layer overgrew on zeolite Y surface protecting the precursor from being further corroded in the reaction solution [22].

N_2 adsorption–desorption results are shown in Table 1. The total surface area of the composites is lower than that of Y zeolite. However, the external surface area of the composites is in the range of 81 and 89 m^2/g, nearly two times that of Y zeolite. The composites also possess larger pore size and considerable pore volume. As shown in Fig. 2, the pore size distributions are centered

Table 1
The structure parameters of HS-FBZ composites.

Sample	S_{BET} (m^2/g)	S_{micro} (m^2/g)	$S_{external}$ (m^2/g)[a]	V_{total} (cc/g)	Average pore size (Å)
Y	845	796	48	0.36	16.8
HS-FBZ-20	692	604	88	0.39	22.5
HS-FBZ-40	703	623	81	0.35	20.1
HS-FBZ-60	715	627	89	0.34	19.0

[a] *t*-plot method.

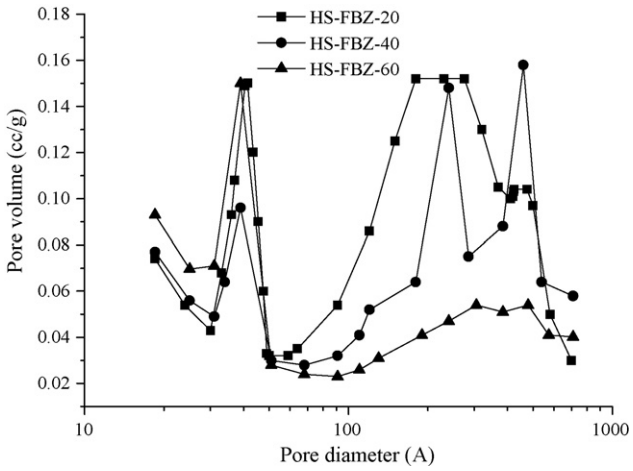

Fig. 2. Pore size distribution of HS-FBZ composites.

around 3.7, 10 and 80 nm, illustrating the existence of meso- and macropores in the composites. This can be attributed to the alkali leaching on Y zeolites and the polycrystalline aggregation of Beta zeolites. During the synthesis, Y zeolite as the precursor was etched by the synthesis solution and the silica in the framework was partially dissolved, causing the enlargement of micropores and resulting in the formation of meso- and even macropores. The polycrystalline aggregation of zeolite Beta around Y zeolite particles also played an important role in the formation of the meso- and macropores in the composites. Among the zeolite composites, HS-FBZ-20 has the largest external surface area and pore volume, as well as average pore size, which are in favor of hydrocracking of bulky molecules.

FT-IR spectra of the composites are shown in Fig. 3, in which the characteristic vibration bands of silica–alumina zeolite can be observed, although the bands position and intensity are not completely identical. The bands at 440–460 cm^{-1} are assigned to the O–T (Si or Al) bending vibrations, the bands at 520–580 cm^{-1} to the double ring external linkage vibrations [23,24], the bands at 740–760 cm^{-1} to the external linkage symmetrical stretching vibrations, and the bands around 1012 cm^{-1} to the internal tetrahedral asymmetrical stretching vibration. Here, a new vibration band appears in the composites and shifts from 1035 cm^{-1} to 1050 cm^{-1} with increasing Beta phase in the composites. The vibration band lies between 1012 cm^{-1} and 1080 cm^{-1}, which are related to Si/Al ratio of the framework of Y and Beta zeolits, respectively, indicating that the Si/Al ratio of the composites is higher than that of Y zeolite, but lower than that of Beta [25]. The new vibration band suggests strongly a new internal tetrahedral asymmetrical stretching vibration appearing in the interface between Y zeolite and Beta zeolite of the composites, implying a variable framework Si/Al ratio in the interface.

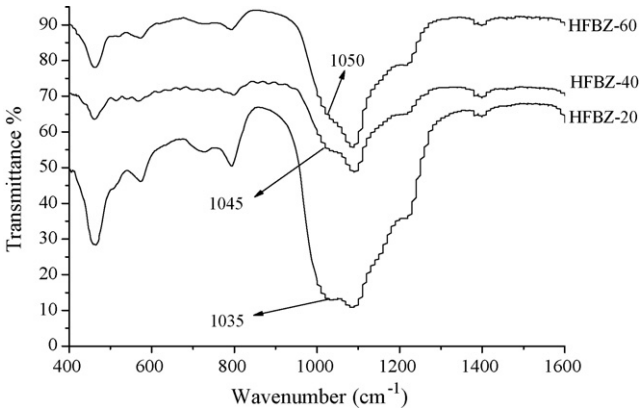

Fig. 3. FT-IR spectra for HS-FBZ composites.

The morphologies of HS-FBZ composites are shown in Fig. 4. It is clear that the morphology of HS-FBZ-20 differs from those of HS-FBZ-40 and HS-FBZ-60. The Si/Al ratios of HS-FBZ-40 and HS-FBZ-60, as determined by X-ray energy dispersive spectroscopy, are 4.7 (Zone "a" in Fig. 4) and 4.3 (Zone "b" in Fig. 4), respectively, which lie between the Si/Al ratios of Y zeolite (2.5) and Beta zeolite (7) [26]. At higher magnification a representative core–shell structure can be observed. In transect of the composite particle showed in Fig. 4 (HS-FBZ) a bigger particle is enwrapped by a thin shell with a thickness of about 80 nm. Y zeolite is no longer an octahedral morphology, but a nearly elliptical particle with smooth surface. The original morphology of Y zeolite particles is found difficultly due to the treatment of alkali. The zeolite Beta shell is composed of laminar polyhedron nano-particles. The SEM observations suggest

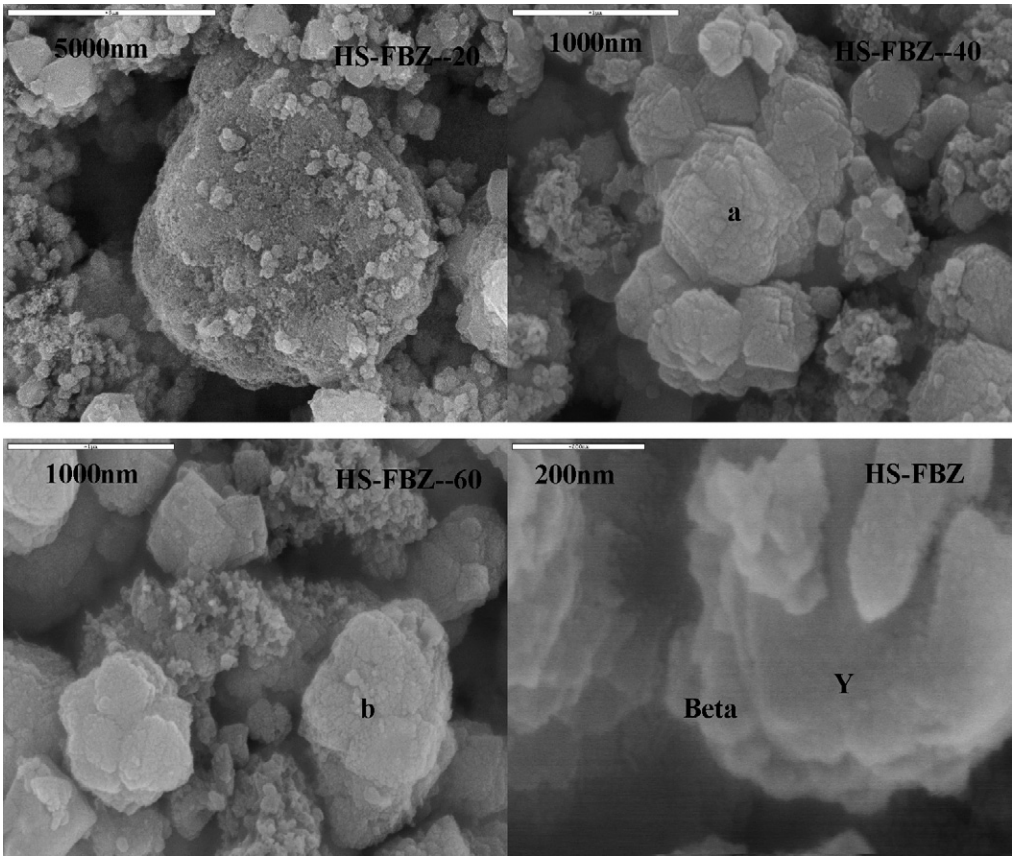

Fig. 4. SEM images of HS-FBZ composites.

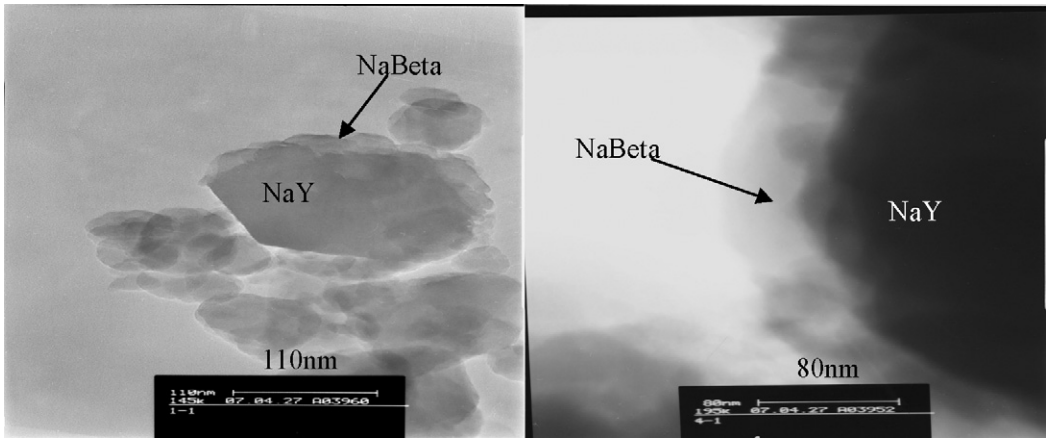

Fig. 5. TEM images of HS-FBZ composites.

the tight joint between core and shell, and no gap between the core zeolite and shell zeolite. This is different from the result reported by Bouizi et al. [27], in which a core–shell zeolite composite has a visible gap between the core zeolite and shell zeolite. The tight joint between the core and shell would result from chemical bond between the core and shell as suggested by image in Fig. 3, in which Si/Al–O tetrahedron possibly twisted resulting in the appearance of vibration peak at 1035 cm^{-1} in FT-IR spectra.

By closer inspection using TEM, we found that the surface of Y zeolite particle is covered by a zeolite Beta layer, giving the composite a core–shell structure. In Fig. 5 the zeolite core with apparent edge and corner at one side can be observed, which is typical of Y zeolite. Clearly the zeolite composite HS-FBZ is composed of two different types of particles, with zeolite Y as the core, and zeolite Beta as the shell. The results from SEM and TEM observations, Si/Al ratio analysis and XRD measurement confirmed the core–shell structure of HS-FBZ zeolite composite, in which zeolite Y was covered by zeolite Beta. The thickness of the shell is estimated as about 80 nm.

The acidity of the zeolite composites was investigated by TPD of ammonia. The NH_3-TPD profiles (Fig. 6) indicate that there are two broad desorption peaks centered around 240 °C and 410 °C, which are assigned respectively to the weak and medium-strong acid sites that can bind with NH_3. The H-form HS-FBZ samples exhibited a similar shape of desorption profile and amount of desorbed NH_3 but different distribution of acid strength. With increasing Beta zeolite fraction in the composite, the high-temperature desorption peaks of NH_3 broadened and shifted to higher temperature. Furthermore, the desorption temperature of the high-temperature peak changed from 360 °C for HS-FBZ-20 to 400 °C for HS-FBZ-40, and to 415 °C for HS-FBZ-60. Obviously the ratio of Beta and Y in the composite has an important influence on the acidity of the composite. The implied significance is that the acidity of the composite can be adjusted by controlling the composition of two zeolites in the composite.

For the investigation of the acid site and acid site distribution, pyridine was selected as a probe molecule because it is the most frequently used base. The FT-IR spectra of pyridine adsorption over the zeolite composites evacuated at 523 K and 623 K are illustrated in Figs. 7 and 8, respectively. The total acid amount (Brønsted and Lewis acids) increases with the increase of Beta phase in the zeolite composites, and HS-FBZ-20 has the lowest total acid amount among the three samples (Fig. 9). HS-FBZ-20 and HS-FBZ-40 have the higher ratio of Lewis to Brønsted acids than HS-FBZ-60 evacuated at 350 °C (Fig. 10). This change is related to the Beta layer on the surface of Y zeolite. The acidity and Lewis/Brønsted ratio of catalysts will play an important role in hydrocracking reactions.

Here, the catalytic performance of the zeolite composites in hydrocracking of VGO was evaluated in a standard micro-activity test unit (MAT), and compared with that of corresponding physical mixture of Y and Beta zeolites. The properties of feedstock and reaction conditions are listed in Table 2 and Table 3, respectively. The hydrocracking product distributions and middle distillate

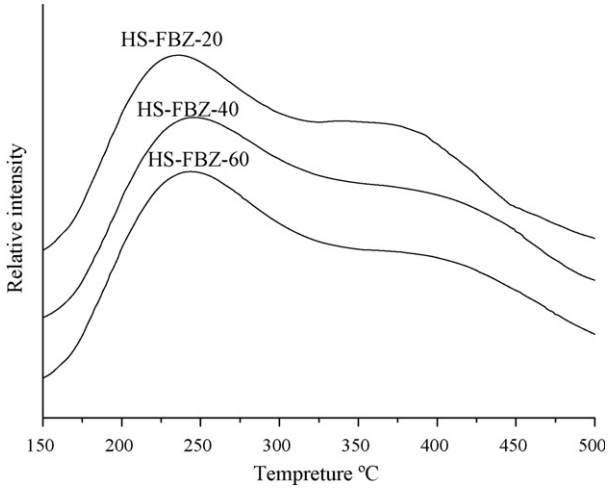

Fig. 6. NH_3-TPD profiles of HS-FBZ composites.

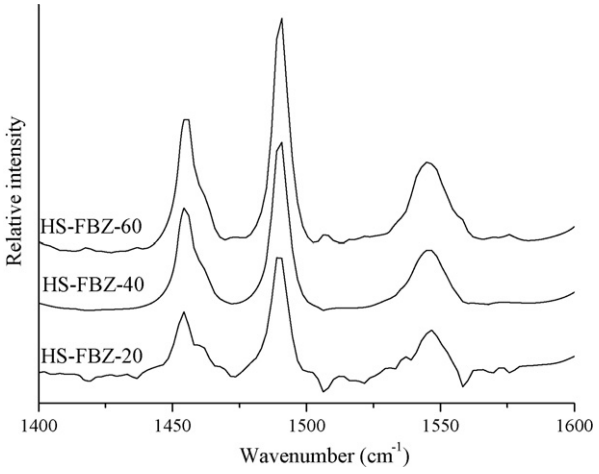

Fig. 7. FT-IR spectra pyridine adsorbed at 250 °C on HS-FBZ composites.

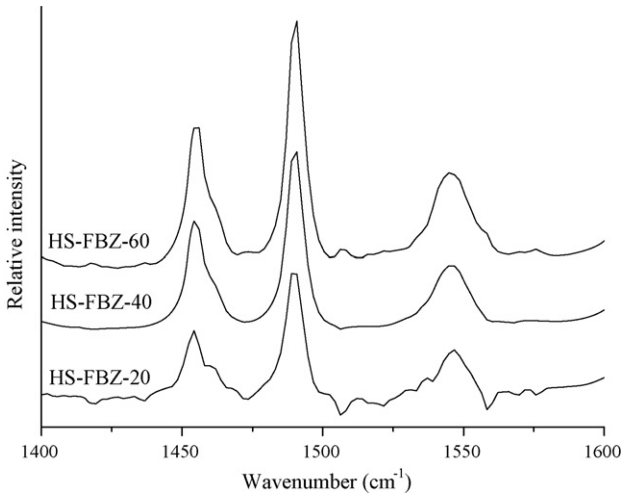

Fig. 8. FT-IR spectra pyridine adsorbed at 350 °C on HS-FBZ composites.

Table 2
Properties of feed oil.

Feed oil	Iran VGO
Density (20 °C), g/cm^3	0.9130
Distillation range, °C	336/542
Coke, wt%	0.39
S, wt%	1.59
N, μg/g	1700
Refractive, η_D^{70}	1.4835
BMCI	45.9

Table 3
Reaction conditions.

Catalysts	Reference	Composite
Hydrogen partial pressure, MPa	15.7	
Hydrogen/oil, v/v	1500:1	
LHSV, h^{-1}	1.5	
Temperature, °C	T	$T-2.5$

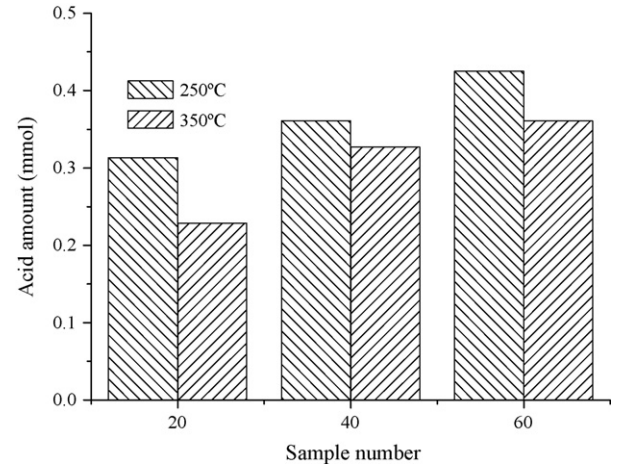

Fig. 9. Total acid amount comparison of composites at 250 °C and 350 °C.

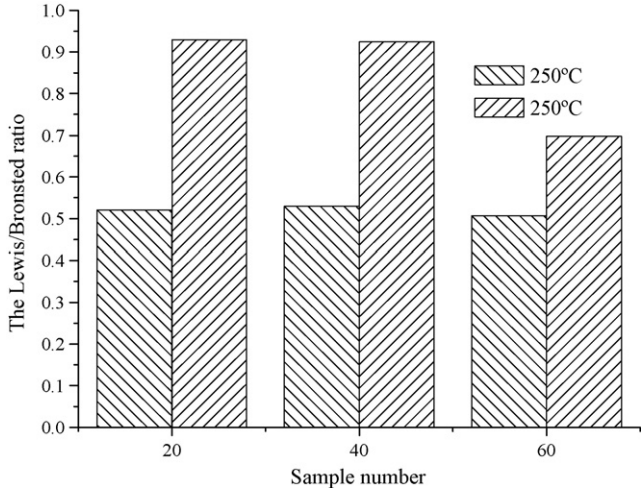

Fig. 10. Lewis/Brønsted ratios of composites at 250 °C and 350 °C.

yields are shown in Figs. 11 and 12, respectively. Compared with the catalyst based on corresponding physical mixture of two zeolites, the catalyst containing HS-FBZ-20 showed the increasing in heavy naphtha yield by 5.61 wt%, jet fuel yield by 11.52 wt%, diesel yield by 2.83 wt% and middle distillate yield by 8.34 wt%. Significantly, the quality of jet fuel and diesel oil over the

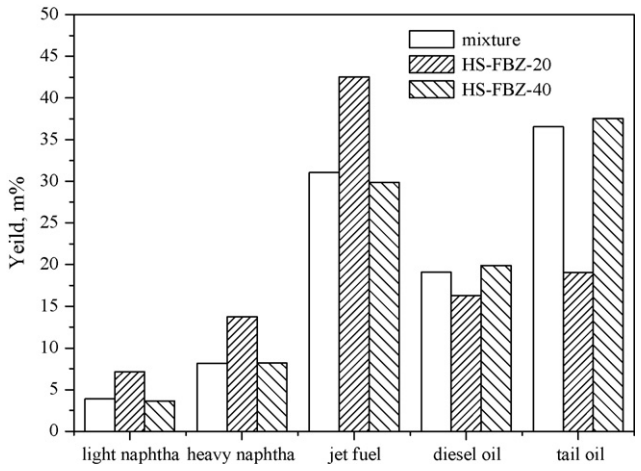

Fig. 11. Hydrocracking product distributions.

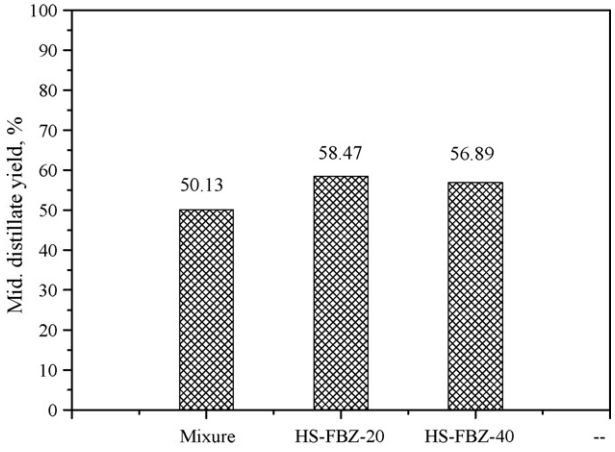

Fig. 12. Middle distillate yields.

Table 4
Properties of different distillates.

Catalyst	Reference	HS-FBZ-20	HS-FBZ-40 [28]
Heavy naphtha			
Density (20 °C), g/cm^3	0.7385	0.7353	0.7403
Aromatization, wt%	60.10	56.01	62.19
Jet fuel			
Density (20 °C), g/cm^3	0.8046	0.7951	0.8111
Freezing point, °C	<−60	<−60	<−60
Smoking point, mm	26	28	26
Aromatics content, vol%	3.4	4.2	6.9
Diesel			
Density (20 °C), g/cm^3	0.8325	0.8239	0.8385
Solidifying point, °C	−4	−14	−8
Cetane number	64.0	76.9	71.05
Tail oil			
Density (20 °C), g/cm^3	0.8452	0.8411	0.8439
Coke, m%	<0.01	0.03	<0.01
BMCI	12.9	13.1	13.5

composite catalysts was better than that over the corresponding mixture (Table 4). For example, aromatic content in jet fuel increased by 0.8 vol%, and solidifying point of diesel oil decreased by 10 °C and cetane index increased by 12.9. Similarly, HS-FBZ-40 also showed higher catalytic activity though its middle distillate yield decreased by 1.58 wt% with respect to HS-FBZ-20.

The above results indicate that the catalysts containing the zeolite composites exhibit higher cracking acitivity in the VGO hydrocracking reaction and produce more distillate products and excellent diesel. The core–shell structure or layered structure of the zeolite composite benefits VGO transformation to heavy naphtha and jet fuel in hydrocracking reaction.

By comparing the catalysts containing HS-FBZ-20 and HS-FBZ-40, the former showed better catalytic performance in VGO hydrocracking process, probably because of its weaker acid strength, lower acid density, better pore diffusion effect and less Beta zeolite. The weaker acid strength and lower acid density are in favor of the transformation of large molecule, thus restraining the further hydrocracking of middle distillate to small molecules [29,30]. On the other hand, the larger pore diameter and pore volume in the composite are helpful to the diffusion of large molecule reactants and various products [31]. The modified pore structure prevents the secondary cracking of the products to smaller molecules. From the cracking point of view, Beta zeolite is a good component for the hydrocracking catalysts, but not a good component for the catalyst for hydroprocessing aimed at maximum production of diesel fuel. Y zeolite is superior to Beta zeolite in developing the catalyst to hydrotreat inferior diesel oil [32]. Based on this standpoint, Y zeolite appears to be more effective in enhancing the hydrotreating activity than Beta zeolite. These considerations rationalize that HS-FBZ-20 gives an enhanced middle distillate yield as a hydrocracking catalyst for treating heavy hydrocarbon feed oil compared with HS-FBZ-40, because it contains less Beta zeolite.

3. Conclusions

HS-FBZ composite zeolite had high surface area, appropriate pore size and volume. SEM and TEM observations as well as IR analysis indicate the characteristics of a core–shell structure of the composite zeolite. The acidity investigation showed the composite has moderate acid sites and adjustable Lewis/Brønsted acid ratio. Compared with the corresponding physical mixture of Y and Beta zeolites, the composite zeolite showed higher activity and middle distillate yield in VGO hydrocracking process, which is due to the interface effect of the bi-phase zeolites in the composite.

References

[1] F. Bataille, J.L. Lemberton, G. Pérot, P. Leyrit, T. Cseri, N. Marchal, S. Kasztelan, Appl. Catal. A: Gen. 220 (2001) 191.
[2] T. Isoda, S. Nagao, X. Ma, Y. Korai, I. Mochida, Sekiyu Gakkaishi 41 (1) (1998) 22.
[3] D. Li, A. Nishishjima, D.E. Morris, G.D. Guthrie, J. Catal. 188 (1999) 111.
[4] S. Bendezu, R. Cid, J.L.G. Firro, A. Lopez Agudo, Appl. Catal. A: Gen. 197 (2000) 47.
[5] N. Kunisada, K. Choi, Y. Korai, I. Mochida, K. Nakano, Appl. Catal. A: Gen. 276 (2004) 51.
[6] D. Solis, T. Klimova, R. Cuevas, J. Ramirez, A. Lopez-Agudo, Catal. Today 98 (2004) 201.
[7] J. Scherzer, Catalytic Materials: Relationship between Structure and Reactivity, ACS Monograph, No. 248, Washington, DC, 1984, p. 157.
[8] Y. Lsaev, J.J. Fripiat, J. Catal. 182 (1999) 257.
[9] G. Garralon, V. Fornes, A. Corma, Zeolites 8 (1988) 268.
[10] A. Corma, V. Fornes, J.B. Monton, A.V. Orchilles, J. Catal. 107 (1987) 288.
[11] J.P. Angevien, M.K. Mitchell, M.S. Oleck, S.S. Shih, US Patent 4,612,108 (1985).
[12] M.A. Ali, T. Tasumi, T. Masuda, Appl. Catal. A: Gen. 233 (2002) 77.
[13] C. Marin, J. Escobar, E. Galvan, F. Murrieta, R. Zarate, H. Vaca, Fuel Process. Technol. 86 (2004) 391.
[14] A. Hassan, S. Ahmed, M.A. Ali, H. Hamid, T. Inui, Appl. Catal. A: Gen. 220 (2001) 59.
[15] P. Wang, B.J. Shen, J.S. Gao, Catal. Commun. 8 (2007) 1161.
[16] H.L. Chen, B.J. Shen, H.F. Pan, Chem. Lett. 32 (2003) 716.
[17] W.P. Guo, L.M. Huang, P. Deng, Z. Xue, Q. Li, Microporous Mesoporous Mater. 44/45 (2001) 427.
[18] Y.P. Li, X.L. Li, Y. Zhang, P.Y. Wen, X.Z. Wang, T. Dou, Y.Z. Xiao, J. Fuel Chem. Technol. 130 (2002) 162.
[19] R. Li, B. Qin, X. Zhang, Q. Guo, W. Sun, J. Ma, A method of preparing bi-microporous zeolite [P], CN200610048273.9.
[20] B. Qin, Q. Guo, X. Zhang, J. Zheng, R. Li, Acta Petrolei Sinica (Petroleum Processing Section) 22 (Suppl.) (2006) 96.
[21] Y. Liu, W. Zhang, T.J. Pinnavaia, J. Am. Chem. Soc. 122 (2000) 8791.
[22] Y. Bouizi, L. Rouleau, V.P. Valtchev, Chem. Mater. 18 (2006) 4959.
[23] G.W. Skeels, D.W. Breck, in: D.H. Olson, A. Bisio (Eds.), Proceedings of 6th International Zeolite Conference, Butterworths, Guildford, 1984.
[24] B.A. Holmberg, H.T. Wang, J.M. Norbeck, Y. Yan, Microporous Mesoporous Mater. 59 (2003) 13.
[25] B.A. Holmberg, H.T. Wang, Y.S. Yan, Microporous Mesoporous Mater. 74 (2004) 189.
[26] H. Lechert, Microporous Mesoporous Mater. 40 (2000) 181.
[27] Y. Bouizi, Loïc Rouleau, Valentin P. Valtchev, Microporous Mesoporous Mater. 91 (2006) 70.
[28] X. Zhang, Q. Guo, Zh. Zhang, F. Ling, W. Sun, R. Li, in: A. Sayari, M. Jaroniec (Eds.), Nanoporous Materials V, World Scientific Publ. Co., Singapore, 2008, p. 99.
[29] P. Mériaudeau, A. Vu, F. Tuan, Lefebvre, T. Vu, C. Nghiem, Naccache, Microporous Mesoporous Mater. 26 (1998) 161.
[30] K. Chao, H. Wu, Li. Leu, Appl. Catal. A: Gen. (1996) 223.
[31] S. Chen, Y. Yang, K. Zhang, J. Wang, Catal. Today 116 (2006) 2.
[32] L. Ding, Y. Zheng, Z. Zhang, Z. Ring, J. Chen, Appl. Catal. A: Gen. 319 (2007) 25.